Corrosion Science 270 (2026) 113993

Contents lists available at ScienceDirect

Corrosion Science

journal homepage: www.elsevier.com/locate/corsci

Niobium and tantalum nitride-based coatings for improved corrosion resistance and conductivity of titanium-based bipolar plates for PEMFCs

Mohammadhossein Johar [a], Yasin Mehdizadeh Chellehbari [a], Leila Moradizadeh [a], Abhay Gupta [a], Xianguo Li [b], Samaneh Shahgaldi [a,*]

[a] Hydrogen Research Institute, Université du Québec à Trois-Rivières, Quebec, Canada
[b] Mechanical and Mechatronics Engineering, University of Waterloo, Ontario, Canada

ARTICLE INFO

Keywords:
Proton exchange membrane fuel cell
Titanium-based bipolar plate
Nitride coatings
Niobium nitride
Tantalum nitride
Corrosion
Interfacial contact resistance

ABSTRACT

Titanium (Ti) is considered as one of the promising substrates for bipolar plates (BPPs) used in proton exchange membrane fuel cells (PEMFCs) due to its resistance to corrosion and low weight. However, its surface undergoes rapid passivation, forming a stable oxide layer that results in high interfacial contact resistance (ICR) with its adjacent components, ultimately degrading cell performance. In this study, niobium nitride (NbN) and tantalum nitride (TaN) coatings were deposited on Ti substrates using magnetron sputtering to suppress passivation and improve conductivity. A thin titanium nitride (TiN) interlayer is pre-deposited to enhance adhesion and prevent delamination. Under harsh accelerated corrosive conditions, TaN coating reduced the corrosion current density and lowered the ICR, fulfilling the 2025 U.S. Department of Energy (DOE) targets for BPPs. Chronoamperometry tests were conducted under conditions simulating PEMFC cathode-side exposure, and at an elevated potential simulating start-up/shut-down and fuel-starvation conditions demonstrated that TaN remained stable and exhibited greater resistance to degradation under both conditions, whereas NbN showed more pronounced degradation. The superior performance of TaN compared to NbN was attributed to its lower electron donor density, as indicated by Mott–Schottky analysis, which reflected the presence of a more stable and less reactive passive film. This finding underscored the critical role of nitride chemistry and electronic structure in governing corrosion and interfacial properties. Overall, the findings established TaN as an effective coating for potential usage to increase the performance, durability, and conductivity of Ti-based BPPs for PEMFCs.

1. Introduction

Hydrogen, as a clean and efficient energy carrier, plays a crucial role in transition from fossil fuels in power generation [1]. Proton exchange membrane fuel cells (PEMFC) are highly efficient at producing electricity from hydrogen gas, offering fast start-up and zero emissions [2]. With their small size, high energy density, low operating temperature, and zero pollution, PEMFCs are suitable for mobility-related applications such as automotive and aerospace systems [3]. Different components in a single cell of PEMFC are shown in Fig. 1. In a PEMFC, hydrogen gas undergoes oxidation at the anode surface of the catalyst-coated membrane (CCM), releasing electrons that flow through an external circuit and protons (H^+) that migrate through the perfluorosulfonic acid (PFSA)-based membrane to the cathode surface. At the cathode, a reduction reaction occurs where these protons and electrons combine with oxygen to form water [4]. On both sides of the CCM, there are gas diffusion layers (GDLs), which have the role of transporting the reactant gases and water removal [5]. Bipolar plates (BPPs) are multifunctional components adjacent to GDLs which have the responsibility of conducting electrical current from cell to cell, distributing reactant uniformly on the catalyst surface, and managing heat and water transport [6].

To ensure the performance and reliability, BPPs must exhibit excellent corrosion resistance, mechanical strength, long-term stability, and

Abbreviations: BPP, Bipolar Plate; CA, Chronoamperometry; CPE, Constant Phase Element; DOE, Department of Energy; EIS, Electrochemical Impedance Spectroscopy; EDX, Energy Dispersive X-Ray Spectroscopy; GDL, Gas Diffusion Layer; ICR, Interfacial Contact Resistance; NHE, Normal Hydrogen Electrode; OCP, Open Circuit Potential; PEMFC, PEM Fuel Cell; PEM, Proton Exchange Membrane; SEM, Scanning Electron Microscopy; SS, Stainless Steel; TA2, Titanium Grade 2; XRD, X-Ray diffraction; XPS, X-ray photoelectron spectroscopy.

* Corresponding author.
E-mail address: samaneh.shahgaldi@uqtr.ca (S. Shahgaldi).

https://doi.org/10.1016/j.corsci.2026.113993
Received 25 March 2026; Received in revised form 27 May 2026; Accepted 31 May 2026
Available online 2 June 2026

superior electrical and thermal conductivity. Hydrophobic surfaces are preferred to enhance water management and facilitate drainage from the cell [7]. Graphite and composite BPPs are generally used for stationary applications with long operational lifespans, however, they are brittle and have low mechanical strength which limits their usage in application with mobility such as automotive technology [8]. Metallic BPPs, on the other hand, can be machined easier than graphite-based BPPs and have higher electrical and thermal conductivity with a lower weight, volume, and cost, therefore, they have attracted more attention from researchers [9]. With proper mechanical properties, such as higher ductility, metallic BPPs are mostly used in motion-oriented applications such as automotive, aerospace and marine. Stainless-steel (SS) is the state-of-the-art material widely used in manufacturing of BPPs regarding its properties like being highly accessible in the market, having high mechanical strength, and possessing exceptional thermal and electrical conductivity. However, SS is prone to localized corrosion in acidic environments like the one exist in PEMFC. Titanium (Ti) is considered as the next generation material and a substitute for SS due to its exceptional resistance to corrosion, lower density, and higher specific strength, making it ideal for reducing system weight in automotive and aerospace applications [10].

Metallic BPPs cannot be used without protective coatings due to multiple reasons. The hydrophilic nature of metallic BPPs can lead to water accumulation, avoiding gas diffusion and disrupting water management [11]. Additionally, under acidic and humid PEMFC conditions and temperature ranging between 60°C - 90°C, they are susceptible to corrosion, which may release metal ions that degrade membrane performance which is considered as common in SS. Furthermore, the formation of passive films, especially on the Ti surface leads to increase in interfacial contact resistance (ICR) between BPPs and the adjacent components, reducing the overall efficiency of the cell [12]. Protective and electrically conductive surface coatings are essential to address mentioned issues and to meet the U.S. Department of Energy's (DOE) targets for 2025, determined for metallic BPPs, requiring a corrosion current density (i_{corr}) below 1 μA.cm^{-2} and ICR below 10 mΩ.cm^2 [13,14].

Niobium (Nb) and tantalum (Ta) as transition metals are known as metals that have significantly high resistance to corrosion and exhibit lower i_{corr} compared to commonly used metals in BPPs such as molybdenum, tungsten, and corrosion-resistant alloys like SS. According to the literature, Nb- and Ta-based coatings are widely recognized as effective materials for enhancing the corrosion resistance as well as the electrical and thermal conductivity of metallic BPPs [15–17]. Transition metals' nitrides have also attracted considerable attention since they are stable chemically and posses acceptable electrical and thermal conductivity [18]. TiN is among the potential coatings for PEMFC BPPs because of their good electrical conductivity. In a study, Li *et al.* applied TiN coating on the surface of Ti using magnetron sputtering and the results showed low i_{corr} around 0.08 μA.cm^{-2}, and the ICR was measured around 4.2 mΩ.cm^2, however the TiN coating thickness was measured 4.15 μm which is considered high compared to the coating applied in present study [19]. The long-term chronoamperometry (CA) test was conducted on this coating and after 12 h the current density was around 65 μA.cm^{-2} which is significantly higher than the DOE target. These results show that while TiN can be a candidate for usage as coating for BPPs in PEMFC, it may still suffer from limited long-term corrosion resistance and surface oxide formation under aggressive PEMFC operating conditions, which can increase ICR during operation. Therefore, in this study, other transition metal nitride coatings, such as NbN and TaN, were investigated to further improve corrosion resistance while maintaining high electrical conductivity and low ICR.

Despite their potential, there are not much research articles exploring the potential of TaN and NbN as protective coatings for Ti-based BPPs in PEMFCs. NbN and TaN coatings are mentioned as highly potential coatings since they have high integrity with balanced conductivity and oxidation resistance [20,21]. This study aims to develop coatings with desirable microstructure which are resistant to corrosion and possess high electrical conductivity to avoid the passivation of Ti substrate and to enhance the stability and performance of the PEMFC stack. To achieve this, TaN and NbN coatings were deposited on Ti substrates using the magnetron sputtering technique as an efficient deposition method. The magnetron generates a magnetic field that ionize the argon gas as the sputtering gas. It efficiently transfers energy to the target, causing atoms to be ejected from the target and deposited

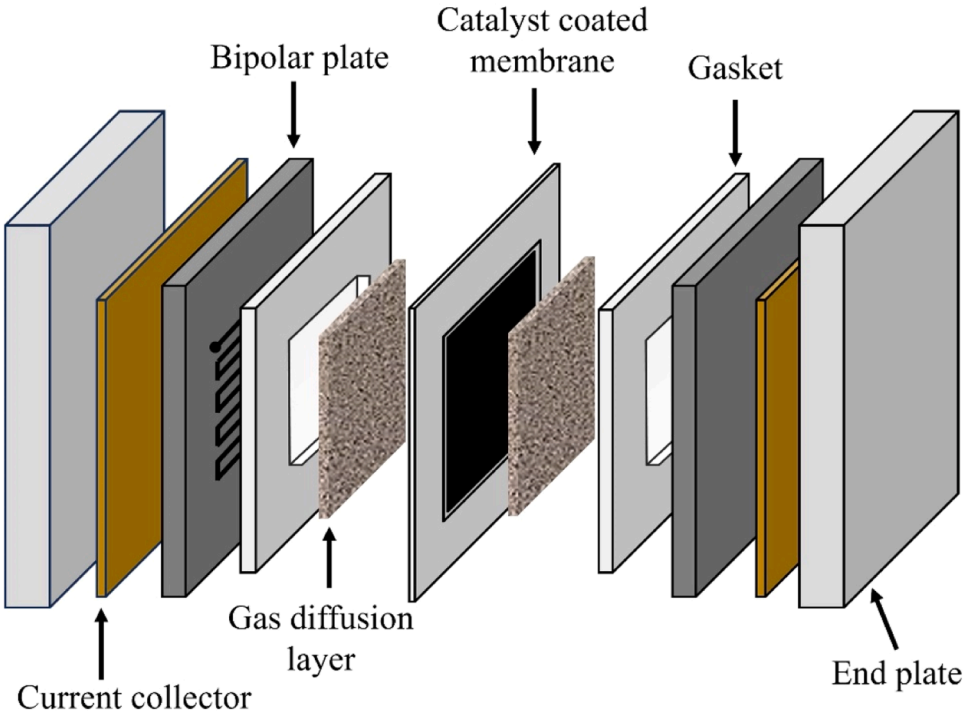

Fig. 1. The schematic of a proton exchange membrane (PEMFC) single cell.

on the substrate to form a thin film [22]. In this study, the physical and electrochemical properties of Ti substrates with and without nitride coatings were investigated using electrochemical measurements such as electrochemical impedance spectroscopy (EIS), potentiodynamic polarization, CA, Mott-Schottky and physical analyses like ICR and contact angle measurements. The aim of these tests is to evaluate the coatings' performance and to determine the best coating configuration for BPP applications within PEMFC environments. While previous studies have investigated Nb- and Ta-based coatings, including multilayer and alloy systems, as well as the optimization of TaN coatings, a direct comparative evaluation of NbN and TaN coatings under similar deposition method with desirable cubic microstructures and a consistent interlayer design remains limited. In this work, NbN and TaN coatings are systematically compared in terms of their corrosion behavior, ICR, and coating stability on Ti substrates. The corrosion protection mechanism and its relation to electrical conductivity of the NbN and TaN coatings are elaborated. Moreover, compared to recent studies on TaN optimization, this work emphasizes a comparative framework that links corrosion behavior, ICR, and coating stability, rather than focusing solely on parameter optimization.

2. Experimental and methods

2.1. Sample preparation and coating procedure

Titanium Grade 2 (TA2), with the chemical composition in Table 1, was used as the substrate. TA2 was used due to a better balance between availability, cost, and mechanical strength while maintaining excellent corrosion resistance which is needed for bipolar plates used in PEMFC [23,24]. 2 cm × 2 cm samples with a thickness of 1.2 mm were mechanically polished using abrasive grinding papers ranging from 1000 to 3000 grit to remove any traces of Ti oxide on the surface [25]. Afterward, the samples were immersed in isopropyl alcohol, rinsed with double-distilled water, and subjected to ultrasonic cleaning for 15 min [26]. The coating was applied using radio frequency (RF) magnetron sputtering with high-purity Ta or Nb targets under a base pressure of 9.0×10^{-5} Pa and a total working pressure of 1 Pa. To ensure a uniform and well-adhered coating, the substrate was rotated at 3 rpm during the process [27]. Before deposition, the substrate was bombarded with argon ions at −800 V bias for 30 min to remove the contaminant and traces of Ti oxide on the surface. A TiN interlayer was deposited at 400 W on the Ti substrate to improve coating adhesion by promoting dense interfacial growth and stronger ion bombardment during deposition. NbN and TaN top layers were subsequently deposited at 300 W [28] and 250 W, respectively, using the Ar/N_2 ratios listed in Table 2 to obtain the desired nitride phases and crystallographic structures. In reactive magnetron sputtering, the applied power strongly influences the energy of sputtered particles, which affects phase formation, preferred orientation, crystallinity, and defect density of nitride coatings [29]. Previous studies have shown that altering sputtering power can modify the preferred orientation and phase evolution of NbN and TaN coatings, particularly promoting the formation of dense face-centered cubic (FCC) δ-phases with improved crystallinity [29,30].

2.2. Physical characterization

The morphological characteristics of the NbN and TaN coatings were analyzed using scanning electron microscopy (SEM) with a Hitachi SU1510 VP SEM. The system was equipped with an energy-dispersive X-ray (EDX) spectroscopy unit and operated at an acceleration voltage of 20 kV. The X-Ray diffraction (XRD) patterns were obtained for all coatings and for the Ti substrate utilizing the New D8 ADVANCE instrument manufactured by Bruker AXS. This analysis employed both Bragg–Brentano geometry with a full scan between $2\theta = 20^\circ - 80^\circ$, employing Cu kα radiation with a wavelength of 1.54 Å at 40 kV and 30 mA. X-ray photoelectron spectroscopy (XPS) spectra were also obtained using a PHI Quantes XPS equipped with an aluminum anode that operates at a photon energy of 1486.6 eV (kα). The cross-section analysis for thickness measurement was conducted using a ThermoFisher Helios 5 UXe Dual Beam Plasma focused ion beam (FIB)-SEM. This method utilizes a focused ion beam to mill a defined cross-section of the coating, followed by high-resolution SEM imaging to measure the thickness. This technique is particularly well-suited for thin coatings, offering precise and localized measurements.

Table 1
Chemical composition of titanium grade 2 (TA2) substrate.

Element	Ti	Fe	O	C	Ni	H
Mass fraction (%)	≥ 98.9	≤ 0.30	≤ 0.25	≤ 0.080	≤ 0.030	≤ 0.015

Table 2
Process parameters including total working pressure while sputtering, Ar gas and N_2 ratio, and deposition power.

Coating	Total Pressure (Pa)	Ar gas (%)	N_2 (%)	Power (W)
TiN	1	90	10	400
NbN	1	85	15	300
TaN	1	80	20	250

As having low ICR is one of the critical properties for BPPs, it was measured through a precise measurement process using a Zwick/Roell GDL tester device under a continuous pressure ranging between 0.5 MPa and 4 MPa for coated and uncoated samples before and after corrosion tests from three separate measurements for each sample (n = 3, p-value < 0.05). In the setup, the samples were placed between two carbon papers, and then two gold-coated copper pistons put pressure on both sides of the assembly [31]. A current of 2.0 A was applied, and the resulting voltage was recorded from the upper gold-coated copper plate.

To measure the contact angle, the Ramé-Hart 100–25-A goniometer, was used. This device dispenses a controlled 5 µl water droplet onto the surface, and an image of the droplet is captured by the goniometer's camera. The software DROPimage processes the image and calculates the contact angle using the circle method, which considers the droplet's height and radius. The measurements were done on 3 different spots on the surface of the samples.

2.3. Electrochemical characterizations

A conventional three-electrode electrochemical setup was used to evaluate the electrochemical behavior of the coated samples. Working electrode was the sample needed to be observed, graphite electrode was employed as the counter electrode, and saturated Hg/Hg_2SO_4 electrode was used as the reference electrode with a potential of 0.680 V versus normal hydrogen electrode (NHE). The solution used for electrochemical analysis was 0.5 M H_2SO_4 at 70 °C to accelerate electrochemical degradation. Before conducting the electrochemical tests, samples were immersed in the solution for 2.0 h in an open circuit potential (OCP) mode for stabilization [32]. Potentiodynamic tests were also carried out at a scan rate of 1.0 $mV.s^{-1}$ at −400 to + 1000 mV versus OCP. In addition, chronoamperometric (CA) testing at 0.2 V vs. Hg/Hg_2SO_4 (0.8 V_{NHE}) for 6 h was selected to investigate an accelerated durability analysis on the coatings which is determined by DOE [16,33–35]. To further evaluate the coating quality, CA was conducted at 0.8 V vs. Hg/Hg_2SO_4 (1.4 V_{NHE}) to simulate harsher conditions that may occur during processes like startup, shutdown, or fuel starvation (when fuel supply is interrupted even when H_2 supply is full), where the cell potential increases and oxidative degradation intensifies. The combined testing strategy led to better evaluation of coating under both stable and dynamic operations [36].

EIS was conducted using an SP300 BioLogic potentiostat, by subjecting the samples to a sinusoidal voltage of 10 mV amplitude at OCP, in a frequency range between 100 kHz and 10 mHz [37,38]. EIS is a powerful analysis being employed to evaluate and compare the effectiveness of corrosion-resistant coatings [39]. Due to significant variability and existence of challenges in producing identical coating samples, this method is generally used in a qualitative or semi-quantitative manner. To facilitate the interpretation of EIS studies, equivalent circuit models are commonly utilized, based on passive electrical engineering and physics principles [40]. Data analysis usually involves nonlinear, complex least squares fitting of these models to the EIS data. However, ongoing debates have arisen over the physical interpretation of the apparent discrepancies observed in the fitted responses of the circuit elements [39,41]. The electrochemical measurements in this work were conducted 3 times to evaluate the consistency of the results to confirm the precision of the tests. The experimental parameters such as solution temperature, electrolyte concentration, etc. were carefully controlled during each electrochemical test to minimize any variation.

Mott-Schottky test was carried out on the NbN and TaN coating after the CA test where a passive film was produced on the surface. With this method the electrical conductivity of the coatings could be compared. The test was conducted in a potential range between −1–0.6 V vs. Hg/Hg_2SO_4 in a specific frequency of 1000 Hz to analyze the characteristics and corrosion resistance mechanism of the semiconductor coatings [42].

3. Results and discussion

3.1. Thickness measurements and surface characterization

The NbN and TaN coatings' thicknesses were measured with FIB-SEM and the measurements are shown in Fig. 2 **(a)** and **(b)** for TiN-NbN and TiN-TaN coatings, respectively. The thicknesses difference is relatively small (less than 10 %) compared to the total coating thickness and is not expected to significantly influence the electrochemical or ICR results [43,44]. In dense nitride coatings, corrosion protection is primarily governed by coating integrity, defect density, and chemical stability rather than minor variations in thickness [45]. Only the top surface is expected to interact with the corrosive medium and after a certain limit, the thickness of coating does not matter if it is passivating [45]. ICR also mostly depends on the surface chemistry and the oxide formation on the surface and the conductivity of the top surface. As shown, a very thin TiN interlayer was properly deposited in both samples to enhance the adhesion of the top layer, which was subsequently coated with NbN and TaN, respectively. TiN aligns well structurally with many transition-metal nitrides such as AlN, CrN, NbN and TaN [46,47]. In addition, since Ti has a high affinity for nitrogen, during the coating process, nitrogen atoms diffuse into the Ti surface and a strong bonding forms which leads to a high adhesion between Ti and the TiN layer [48,49] and due to the dense nucleation of the deposited material, the TiN structure is found to be compact and homogeneous [50]. The TiN interlayer is also expected to reduce surface roughness which results in a denser and smoother top coating resulting in higher resistance to ion diffusion from the solution to the surface of the Ti substrate, and lower ICR [51]. Based on these considerations, the TiN interlayer is expected to contribute to improved coating integrity and adhesion, as reported in the literature. However, the role of the interlayer is not the focus of this study, and its effect is interpreted qualitatively. The differences further observed in this study between NbN and TaN coatings, particularly in terms of delamination behavior, therefore arise from a combination of factors, including coating microstructure, electrical conductivity, and intrinsic electrochemical stability, rather than being attributed solely to adhesion effects. The XRD patterns of NbN and TaN coatings on TiN interlayer in Fig. 3, confirm the successful formation of crystalline nitride phases. NbN coating exhibits characteristic peaks at approximately 35.1°, 41.7°, 60.5°, 70.5°, and 74.3° which can be related to (111), (200), (220), (311), and (222) planes of the face-centered cubic (FCC) δ-NbN phase, respectively. The diffraction pattern of the TaN coating also shows distinct peaks at 35.8°, 41.6°, and 60.2°, which correspond, in order to (111), (200), and (220) planes of the cubic δ-TaN phase. In both samples, Ti substrate shows visible peaks, especially near 38.4° and 40.2°, since the coatings are thin, and X-Ray penetration occurs through the coating to the substrate. The XRD results proved that both NbN and TaN coatings were successfully developed in a stable FCC (NaCl-type) structure, which is known to provide high electrical conductivity and chemical stability with reduced internal stress in the structure [52,53]. These properties contribute to improved corrosion resistance and low ICR, making them suitable for protective coatings on titanium BPPs in PEMFCs.

3.2. Electrochemical analyses

EIS test was conducted on the Ti substrate before and after applying NbN and TaN coatings. The Nyquist plots provided in Fig. 4 **(a)** revealed two capacitor loops for Ti substrate without coating. The existence of two capacitor loops indicates that the passive film formed on the surface is porous and significantly damaged [54]. The low-frequency and high-frequency capacitor loops are related to the dissolution of the oxide film on the Ti surface (slower process), and the electrical double layer at the interface between the passive layer and the solution, respectively [37,55]. The Nyquist plot for TaN coating exhibited the largest semicircle, indicating the highest charge transfer resistance (R_{ct}) and superior electrochemical stability. NbN coating displayed a semicircle with smaller diameter, showing lower corrosion resistance compared to TaN. Ti substrate exhibited the smallest semicircle, indicating poor R_{ct} and higher tendency to degradation. Higher frequency region is magnified and shows the significantly lower impedance of the uncoated Ti substrate. These results indicate that TaN formed a highly protective passive film which prevented the charge transfer providing better resistance to corrosion-related degradation.

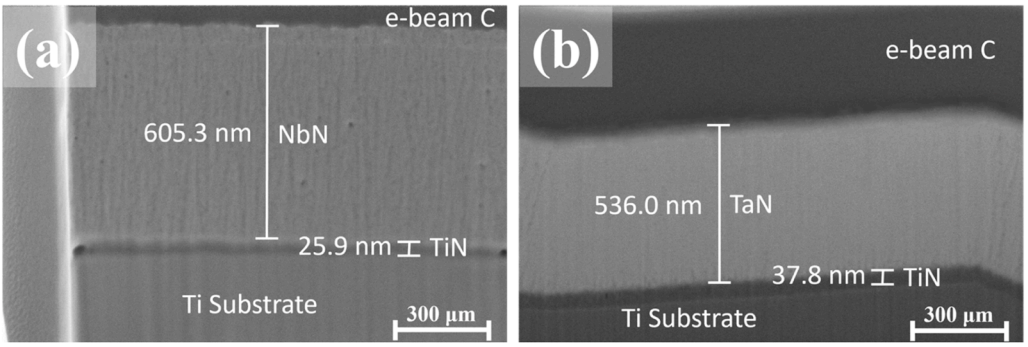

Fig. 2. Cross-section micrographs of **(a)** TiN-NbN and **(b)** TiN-TaN coatings, indicating thickness of each layer by focused ion beam (FIB)-SEM.

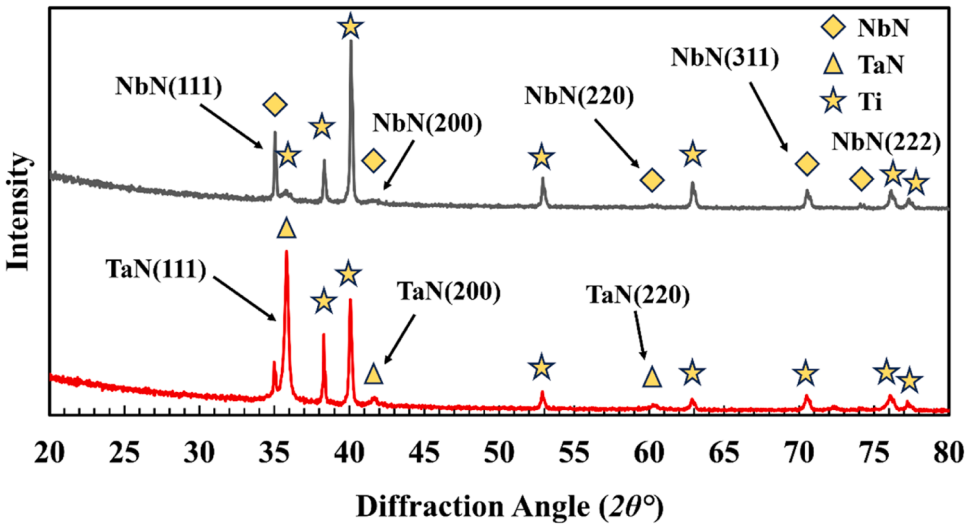

Fig. 3. X-Ray diffraction (XRD) patterns of NbN and TaN coatings on the surface of Ti substrate.

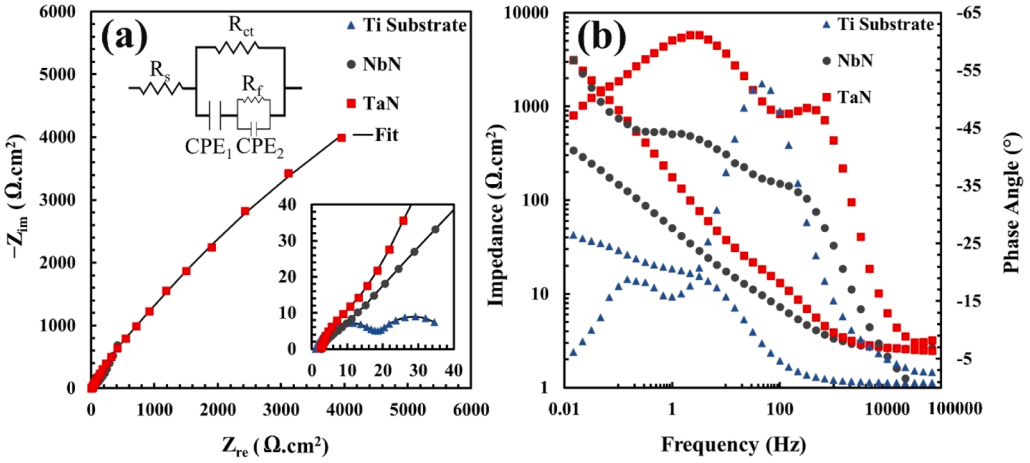

Fig. 4. **(a)** Nyquist and **(b)** frequency-phase angle plots for titanium (Ti) substrate, NbN, and TaN coatings.

The Bode plots provide insight into the electrochemical behavior of the coatings by recording the impedance magnitude (|Z|) and the phase angle versus frequency. The Bode plot for TaN coating in Fig. 4 **(b)** confirms that this coating posses the highest impedance in all of the frequencies exhibiting its superior protection against the penetration of the electrolyte. NbN demonstrates a moderate impedance response, while the Ti substrate exhibits the lowest impedance, suggesting weak corrosion resistance. The phase angle plot for TaN has an angle between 55° to 65° in a broad frequency range that is relatively high which shows a sign of capacitive behavior and a stable passive layer that inhibits charge transfer. NbN had a lower phase angle indicating partial capacitive behavior, whereas Ti displays a resistive response with a very low phase angle of around 10°, suggesting poor protection on the surface. These findings highlight that the TaN coating effectively impedes charge transfer and prevents electrolyte interaction with the substrate, while NbN offers moderate protection.

An equivalent electrical circuit model with solution resistance (R_s), R_{ct}, film resistance (R_f), and a constant phase element (CPE) to account for non-ideal capacitive behavior, was chosen. The equivalent electrical circuits for samples with single and double time constants with fitted lines are provided in Fig. 4 **(a)** and the extracted parameters are provided in Table 3. The fitting error (χ) between the experimental data and the fitted model was below 1% for all samples, indicating a satisfactory level of fit. A CPE is used to model the surface capacitance of the coating, accounting for the non-uniformity and irregularity of the coating surface or passive film [56–60]. The impedance of the CPE is expressed as follows:

$$Y = Y_0 \quad (j.\omega)^n \tag{1}$$

where Y_0 represents the constant admittance, $j^2 = -1$, ω denotes the frequency, and n is an exponent typically ranging between 0 and 1.

Table 3
Fitting results of impedance spectra for the corrosion of Ti substrate and coated samples in 0.5 M H_2SO_4 electrolyte at 70 °C.

Sample	R_s (Ω.cm^2)	CPE$_1$ (F.cm^{-2})	n_f	R_f(Ω.cm^2)	CPE$_2$ (F.cm^{-2})	n_f	R_{ct} (Ω.cm^2)	$R_P(R_f + R_{ct})$(Ω.cm^2)	χ(%)
Ti Sub	1.1	7.1×10^{-2}	0.89	38.6	1.8×10^{-3}	0.92	18.5	57.1	0.9
NbN	1.0	3.9×10^{-2}	0.91	19.1	1.1×10^{-3}	0.97	1450.4	1471.1	0.8
TaN	1.8	1.4×10^{-3}	0.89	2.7	8.4×10^{-4}	0.88	12009	12012	0.8

$R_f$is the resistance of the passive film or the resistance in coating-solution interface which shows the ability of the coating as a barrier against the diffusion of corrosive ions from the solution through the coating [61]. A stable passive film possesses a higher R_f value with higher protective properties which can effectively reduce the rate of corrosion [62]. The fitting results confirmed that TaN has the highest R_{ct}, showing superior electrochemical stability, whereas NbN exhibited moderate values, offering some level of protection, however, may require further optimization for use in highly aggressive environments. Polarization resistance (R_P) is the sum of the R_{ct} and R_f. For the TaN coating, the combination of low R_f and higher R_{ct} has a physical interpretation and a lower R_f indicates the presence of a thin passive layer with conductive properties while high R_{ct} shows slow charge transfer at coating/electrolyte interface, explaining that despite having lower film resistance, it significantly suppresses corrosion reactions by limiting charge transfer processes. Ti substrate, in contrast, demonstrated the lowest R_{ct} and least capacitive behavior, confirming its poor corrosion resistance. TaN coating on Ti substrate significantly enhanced its electrochemical stability which can result in improving the longevity and performance of Ti-based BPPs in harsh operating conditions.

Before applying potentiodynamic polarization tests, it is necessary to keep the samples in the solution under OCP for a period to become stable. This ensures the accuracy and repeatability of the electrochemical measurements. In this study, samples were immersed in the electrolyte solution for 2 h, which was sufficient to reach a stable OCP [63], indicating that equilibrium between the sample surface and the electrolyte had been established, as illustrated in Fig. 5 **(a)**. OCP analysis offers valuable insights into the thermodynamic tendency of a material to corrode in each environment. A higher (more noble) OCP suggests enhanced corrosion resistance, whereas a lower (more active) OCP implies increased vulnerability to corrosion. According to the OCP results, the TaN coating exhibited the highest OCP value compared to Ti substrate and NbN coating, indicating superior electrochemical stability and corrosion resistance. Ti substrate shows the lowest OCP values, and the sharp OCP drop suggests the breakdown of their passive protective films, making them more prone to corrosion.

Potentiodynamic polarization tests are necessary for evaluating the electrochemical behavior and to analyze the stability and corrosion resistance of coated and uncoated Ti substrates in terms of corrosion potential (E_{corr}) and corrosion current density (i_{corr}) [64,65]. Such insights are crucial in selecting materials and in designing effective corrosion protection approaches. Tafel plots are shown in Fig. 5 **(b)** and the data are extracted from the plots can be seen in Table 4. The anodic branch for Ti substrate reveals distinct regions including active dissolution, active-passive transition, and trans-passive, with noticeable fluctuations indicating an unstable passive film. The points near −0.7 and −0.5 V vs. Hg/Hg_2SO_4 are attributed to changes in the oxide layer, indicating oxide formation, partial breakdown or thinning, and repassivation of the bare material when becoming exposed to the solution again [66]. These fluctuations confirm the instability of the titanium oxide layer under the tested condition. NbN demonstrates a more stable passive behavior compared to Ti with a reduced passive current plateau and a lower i_{corr} of 34.3 μA.cm^{-2}. More positive E_{corr} shows more electrochemical stability for TaN compared to NbN and Ti substrate. Although TaN coating does not exhibit full passivation behavior, and its anodic current density gradually increases with increasing the potential. This suggests that the TaN coating provides a barrier effect rather than forming a self-repairing passive film like conventional passive materials. This coating shows the lowest i_{corr} (0.8 μA.cm^{-2}), implying superior protection and higher resistance to electrochemical degradation.

Table 4
Electrochemical parameters obtained from potentiodynamic polarization curves.

Sample	E_{corr} (mV)	i_{corr} (μA.cm^{-2})	β_a (mV)	β_c (mV)
Ti Substrate	−1008.3	376.2	66.0	99.0
NbN	−635.6	34.3	476.5	66.0
TaN	−433.5	0.8	300.1	171.2

The chronoamperometry (CA) test results accompany the potentiodynamic results by assessing the stability of the passive films over time at a fixed potential [67,68]. The CA tests were conducted at a constant potential of 0.2 V vs. Hg/Hg_2SO_4 or + 0.8 V_{NHE} to simulate the oxidative environment at the cathode side of PEMFCs based on DOE target [69]. This test provides information on the coatings' electrical conductivity, adherence to the substrate, and any potential interactions with the electrolyte or reactants present in the fuel cell environment [70]. In Fig. 6 **(a)**, the Ti substrate exhibited an unstable passivation behavior, and the current density decreased from higher to lower values showing continued dissolution and passivation of Ti during the time [16,71]. In contrast, NbN shows a relatively stable current density, suggesting moderate protection but some degree of passive film degradation. TaN demonstrates the most stable passivation behavior and resistance to corrosion by exhibiting lowest current density during the time. The current density for TaN and NbN coating after 6.0 h corrosion process was measured around 0.67 μA.cm^{-2} and 7.93 μA.cm^{-2}, respectively. The current density for TaN was less than 1.0 μA.cm^{-2} (DOE target for BPPs determined for 2025), making it as a promising candidate for corrosion protection in aggressive environments.

As mentioned earlier, the normal operating potential of a PEMFC

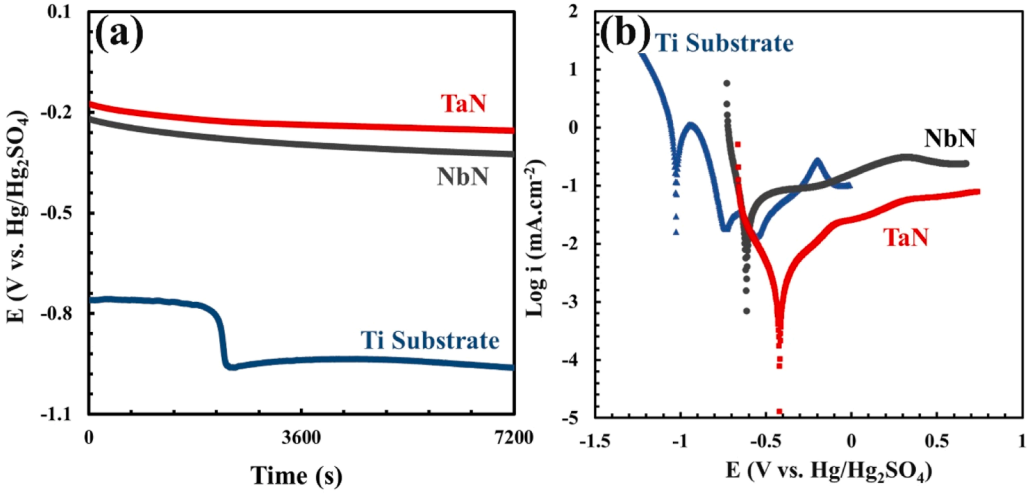

Fig. 5. **(a)** Open circuit potential, and **(b)** potentiodynamic polarization plots for NbN and TaN coatings compared to titanium (Ti) substrate.

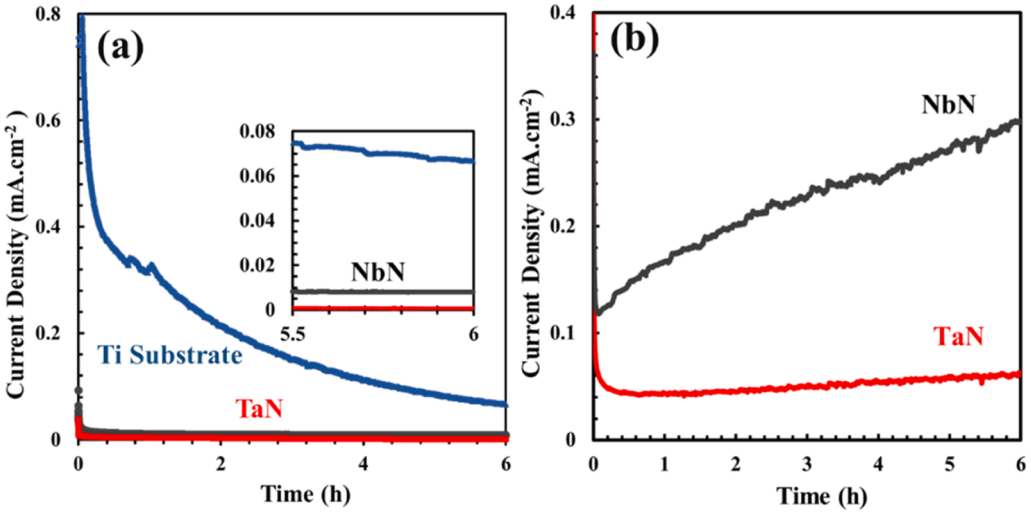

Fig. 6. Chronoamperometry (CA) plots for NbN and TaN coatings compared to titanium (Ti) substrate at **(a)** 0.2 V vs. Hg/Hg_2SO_4, and **(b)** at 0.8 V vs. Hg/Hg_2SO_4.

cathode is roughly 0.2 V vs. Hg/Hg_2SO_4; yet during unavoidable transients such as start-up, shut-down, or brief fuel-starvation events, the potential can surge to 1.3–1.6 V_{NHE} [15,72]. These short-duration voltage spikes accelerate surface oxidation, metal dissolution, and nitrogen loss, thereby shortening the service life of metallic or nitride-coated BPPs. To evaluate coating durability under harsh electrochemical excursions, NbN- and TaN-coated Ti BPPs were subjected to a 6.0 h CA test hold at 0.8 V vs. Hg/Hg_2SO_4 which is within the range of 1.3–1.6 V compared to NHE (Fig. 6 **(b)**). This test is intentionally more severe than typical operating conditions and offers a stringent measure of long-term coating durability [36]. Upon applying the potential, NbN coating exhibited an initial increase in current density due to the rapid oxidation of surface. This increase in current density for the TaN coating was not significant and stabilization occurred at approximately 0.05 mA.cm^{-2}. The current density remained nearly constant, showing only a slight increase to about 0.06 mA.cm^{-2}, indicating excellent stability under sustained oxidative conditions. In contrast, the current density for NbN increased throughout the test, ultimately exceeding 0.30 mA.cm^{-2}. This gradual rise showed progressive degradation of the protective film due to the existence of defects and porosities in the passive, which leads to repeated breakdown and re-passivation processes under high potential stress.

The superior resistance to corrosion of TaN coatings is attributed to both thermodynamically stability and favorable kinetic behavior. In potentials more than 0.8 V vs. Hg/Hg_2SO_4, TaN tends to form a dense and stable tantalum oxide (Ta_2O_5 or TaO_xN_y), which acts as a barrier against ion transport and the penetration of the solution [73–75]. In contrast, niobium nitrides become susceptible to degradation at high voltages. NbN can undergo partial oxidation when nitrogen is depleted, leading to the formation of a more porous and defect-rich Nb_2O_5 layer [76]. This transformation of the nitride coating to defect-rich passivation layer results in deeper diffusion of the acidic solution through the coating, accelerating anodic dissolution. While the current densities at 0.8 V vs. Hg/Hg_2SO_4 do not meet the U.S. DOE's i_{corr} of 1 μA.cm^{-2}, which is due to the extremely harsh conditions, the significant gap between TaN and NbN illustrates the superior durability of TaN.

By combining the CA results in two different potentials, it can be concluded that TaN outperforms NbN based on presenting stable behavior, making it the most suitable coating for titanium-based BPPs. The test at 0.8 V vs. Hg/Hg_2SO_4 confirms that TaN offers superior protection in highly corrosive conditions, which is essential for the stop-start dynamics typical of PEMFC systems.

TaN generally exhibits n-type semiconducting behavior based on the literature [77,78], with a relatively high concentration of free electrons. From a qualitative perspective, this electron-rich character may influence surface electrochemical processes by affecting the tendency for oxidation and passive film formation. The n-type semiconducting nature of TaN tends to suppress oxidation reactions due to the high concentration of free electrons. This electronic structure may promote the formation of stable passive layers, which may reduce anodic dissolution processes. This reduces metal ion release and improves the corrosion stability. The significantly lower i_{corr} and more positive E_{corr} for TaN suggest that it provides the best protection among the tested samples [79,80]. The lower i_{corr} indicates improved corrosion resistance. This may be related to changes in defect structure (e.g., oxygen vacancies) and electronic properties; however, these aspects are inferred and would require further characterization for direct confirmation. The schematic image in Fig. 7 is therefore intended only as a qualitative representation of this concept, showing TaN as an n-type material with a higher density of electrons in the conduction band (i.e., the energy range in which electrons are delocalized and contribute to electrical conduction). Within this simplified framework, the electronic structure of TaN may contribute to more stable passive film formation and reduced anodic activity during polarization. However, this interpretation is not based on a quantitative Mott–Schottky analysis in the present work and should not be considered as a direct extraction of semiconductor parameters. Similarly, differences observed for NbN coatings are discussed in a qualitative manner, as their electronic properties can vary significantly depending on composition, stoichiometry, and microstructure [81]. These variations can influence charge transport and surface reactions, potentially leading to less stable passive film formation and higher current densities observed in the polarization curves. The semiconductive behavior of the nitride coatings was analyzed by Mott-Schottky measurements (Fig. 8) using the below equation:

$$C^{-2} = 2 \quad (\varepsilon\varepsilon_0 N_D)^{-1}(E - E_{fb} - KTe^{-1}) \tag{2}$$

where, C represents semiconductor electrode under depletion condition, e is the electron charge, K is Boltzmann's constant, E is the applied electrode potential and E_{fb} is the flat band potential, ε_0 the vacuum permittivity, ε the relative dielectric constant of the semiconductor, T is the absolute temperature, and N_D is the donor density for n-type coatings. Since NbN and TaN have different properties, the ε for them is different and can be measured with this formula:

$$\varepsilon = Cd/\varepsilon_0 A \tag{3}$$

where, d is the dielectric thickness and A is the surface area. By calculating the linear region's slope (m) in the Mott-Schottky plot, and from

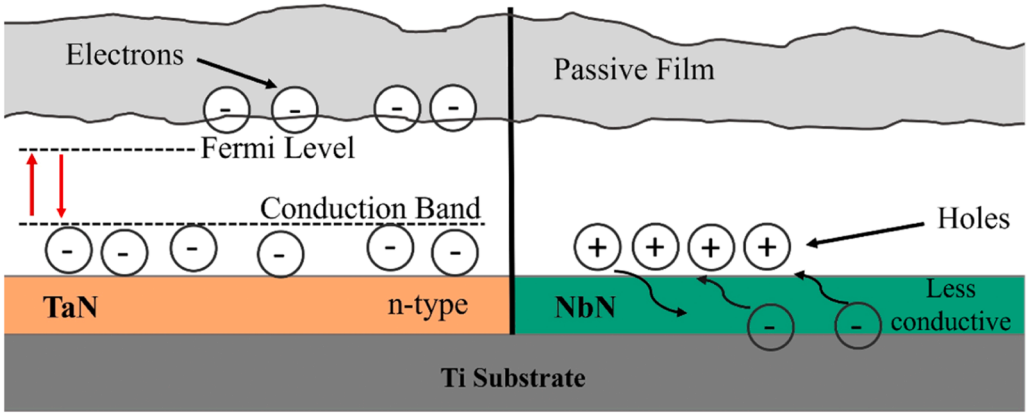

Fig. 7. Schematic illustration of the proposed corrosion behavior of TaN and NbN coatings, highlighting differences in electronic properties and their possible influence on corrosion resistance.

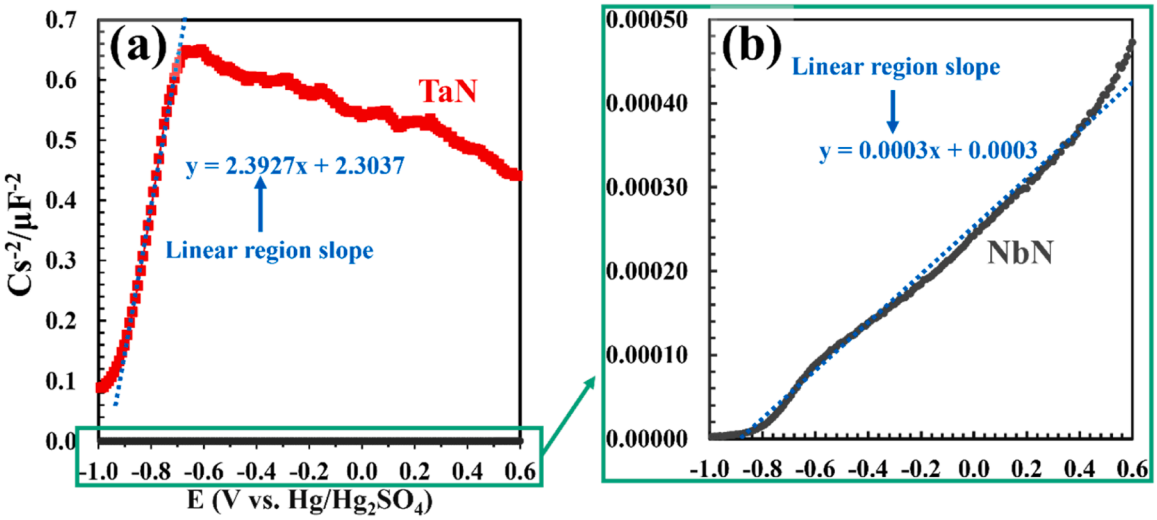

Fig. 8. **(a)** Mott-Schottky plots for NbN and TaN coatings, **(b)** zoom-in for NbN plot.

the below formula, N_D can be measured for NbN and TaN coatings:

$$N_D = \quad 2 \quad (\varepsilon\varepsilon_0 em)^{-1} \tag{4}$$

By measuring the N_D for TaN and NbN coatings, the value is significantly higher for NbN compared to TaN. Lower N_D indicates the fewer holes or oxygen vacancies, which results in denser passive layer with superior protective properties [82].

It must be noted, however, that the electronic properties of transition metal nitrides are highly sensitive to factors such as stoichiometry, microstructure, and the presence of oxide/nitride phases. The above discussion is intended as a qualitative interpretation. The improved corrosion resistance of TaN observed in this work is more reliably attributed to its higher chemical stability, denser morphology, and the formation of a more stable passive layer under PEMFC conditions, while electronic structure effects are considered a secondary contributing factor.

3.3. Morphology and chemical composition analysis of coatings

The SEM micrographs provided a comparative view of the surface morphology of TaN and NbN coatings both before CA (BCA) and after CA (ACA). For TaN coating, Fig. 9 **(a)** shows a smooth and dense surface with no obvious defects and cracks, even at higher magnification in Fig. 9 **(b)**. After corrosion, as seen in Fig. 9 **(c)** and **(d)**, the TaN surface remained intact. While some surface roughening and fine scratches were observed, there was no evidence of severe degradation such as pitting, cracking, or delamination. This demonstrates that TaN offered excellent corrosion resistance, likely due to the formation of a stable passive layer that hindered the access of aggressive species. In contrast, NbN coating showed a significantly different behavior. Fig. 9 **(e)** and **(f)** reveal a rougher and more heterogeneous surface even before corrosion, with visible microcracks and uneven features. According to the literature, NbN coatings deposited by magnetron sputtering can commonly exhibit columnar structure during growth, which may lead to increased surface roughness and non-uniformity. Such features are also influenced by shadowing effects inherent to sputtering processes, which can further amplify surface roughness and heterogeneity [83]. These imperfections act as initiation points for corrosion. After CA test, in Fig. 9 **(g)** and **(h)**, an extensive damage to the surface coating including crack propagation and delamination is evident, indicating that the coating failed to maintain its protective function. This severe degradation suggests that NbN either did not have the ability to form a stable passive or if the passive film was formed, it rapidly broke down in corrosive condition. This degradation may also be partially related to the relatively lower electrical conductivity of NbN, where hole carriers at the surface could facilitate electrochemical oxidation reactions. Nevertheless, the corrosion behavior likely results from the combined influence of coating morphology, microstructural defects, electrical properties, and intrinsic electrochemical stability. The porous and fragmented morphology seen after corrosion further indicates poor coating cohesion and structural

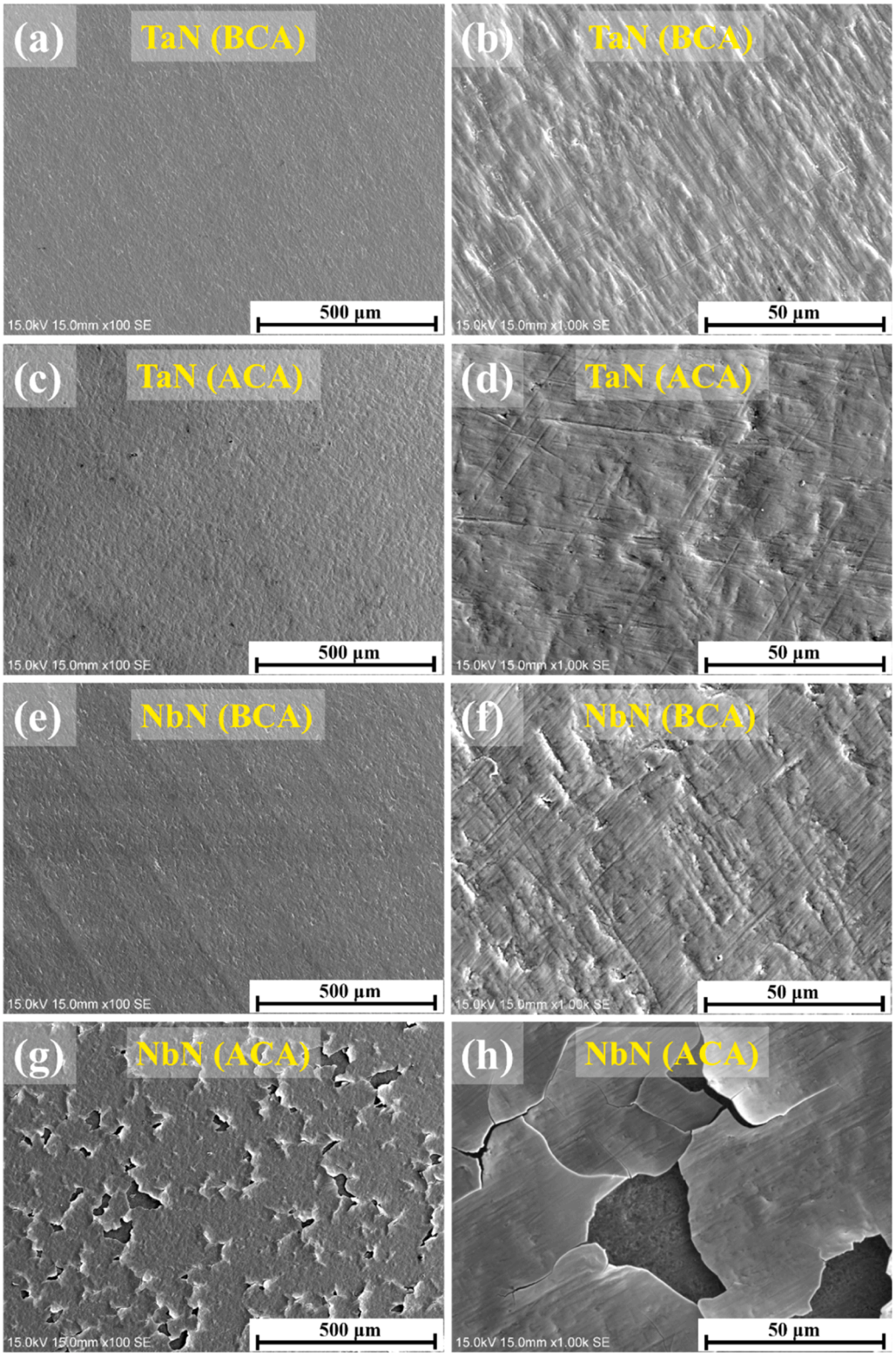

Fig. 9. SEM morphological micrographs for **(a, b)** TaN before CA, **(c, d)** TaN after CA, **(e, f)** NbN before CA, **(g, h)** NbN after CA, showing extreme coating detachment of NbN coating after CA.

resilience.

TaN showed superior corrosion resistance because of its higher chemical stability and the formation of a denser, more stable Ta_2O_5 passive layer compared to the more porous and defect-rich Nb_2O_5 layer. Therefore, the enhanced corrosion resistance of TaN is not solely attributed to differences in the initial coating morphology, but also to the inherently superior stability and protective nature of the Ta passive film. The preservation of surface integrity under corrosive conditions was consistent with TaN's reported n-type semiconducting behavior, where the presence of excess electrons could suppress anodic dissolution by lowering the availability of holes, facilitating passive film stabilization [84,85].

Fig. 10 shows high-resolution XPS spectra of the Nb 3d and Ta 4 f regions for NbN- and TaN-coated Ti-based BPPs before and after six hours of CA, revealing the surface chemical evolution of the nitride coatings under harsh electrochemical conditions. Before CA (Fig. 10 **(a)** and **(c)**), the Nb 3d spectrum can be fitted into NbN (~204.2–205.6 eV, 31.85 at%), NbO_2 (~206.0–206.8 eV, 18.44 at%), and Nb_2O_5 (~206.9–210.2 eV, 49.87 at%), indicating partial surface oxidation of the NbN layer. The Ta 4 f spectrum consists of TaN (~23.5–25.0 eV, 54.44 at%), Ta–N–O (~25.2–26.0 eV, 12.36 at%), and oxidized Ta species (~26.0–26.8 eV, 33.20 at%), which are attributed to Ta_2O_5 as the dominant oxide phase. These assignments are consistent with previous reports for NbN and TaN coatings.

After 6 h of CA in 0.5 M H_2SO_4 at 70 °C (Fig. 10 **(b)** and **(d)**), both coatings exhibit further oxidation, although to different extents. For the Nb coating, the NbN fraction decreases to 16.29 at%, while NbO_2 and Nb_2O_5 increase to 28.99 at% and 54.72 at%, respectively, indicating progressive oxidation of Nb–N bonds toward higher oxidation states. In contrast, the Ta 4 f spectra show comparatively smaller changes. Although an increase in oxide contribution is observed after polarization, the overlap between Ta–N and Ta–O components introduces some uncertainty in the quantitative analysis. For consistency, all spectra before and after CA were analyzed using identical fitting constraints with 4 at% uncertainty, background subtraction procedures, and sensitivity factors, allowing for a meaningful comparison of relative changes in atomic fractions. It should be noted that XPS is a surface-sensitive technique, probing only the top ~5–10 nm of the coating. Therefore, the results primarily reflect the composition of the outermost reacted layer rather than the entire coating thickness. The observed increase in oxide species indicates the formation of a surface oxide layer during polarization, while the underlying nitride layer may remain largely intact.

Overall, the XPS results demonstrate that both coatings undergo partial surface oxidation under acidic, high-temperature conditions, forming Nb_2O_5 and Ta_2O_5 surface layers. However, the extent of oxidation is more pronounced for NbN than for TaN. The relatively smaller change in TaN-related signals suggests a more limited degree of surface transformation, consistent with the higher stability of Ta–N bonds, rather than implying that the coating remains entirely unchanged.

3.4. Interfacial contact resistance

ICR measurements were performed on the Ti substrate and coated samples before and after the CA test to assess the electrical contact resistance between the samples and the GDL across a pressure range of 0.5–4 MPa. ICR measurement provides valuable insights into optimizing coatings with the aim of minimizing contact resistance between components. For all the samples, the ICR decreased with increasing compaction force which is because of the increased contact area between the samples and the GDLs [86]. At 1.5 MPa, as the actual compaction force in PEMFCs [87,88], the performance of the Ti substrate, NbN, and TaN coatings before and after corrosion showed significant differences both before and after CA test as shown in Fig. 11. Ti substrate exhibited a contact resistance of 14.2 $m\Omega.cm^2$ which can be considered as a low contact resistance. However, after CA, the ICR raised to 38.6 $m\Omega.cm^2$, likely due to the thickening of the TiO_2 layer, indicating poor conductivity for applications requiring high electrical conductivity. This presents a significant challenge when using uncoated Ti substrates in PEMFCs [89,90]. In contrast, NbN demonstrated improved conductivity compared to the Ti substrate. Before CA test, the ICR was measured around 8 $m\Omega.cm^2$, suggesting that NbN effectively reduced contact resistance, however, after corrosion, the ICR increased to around

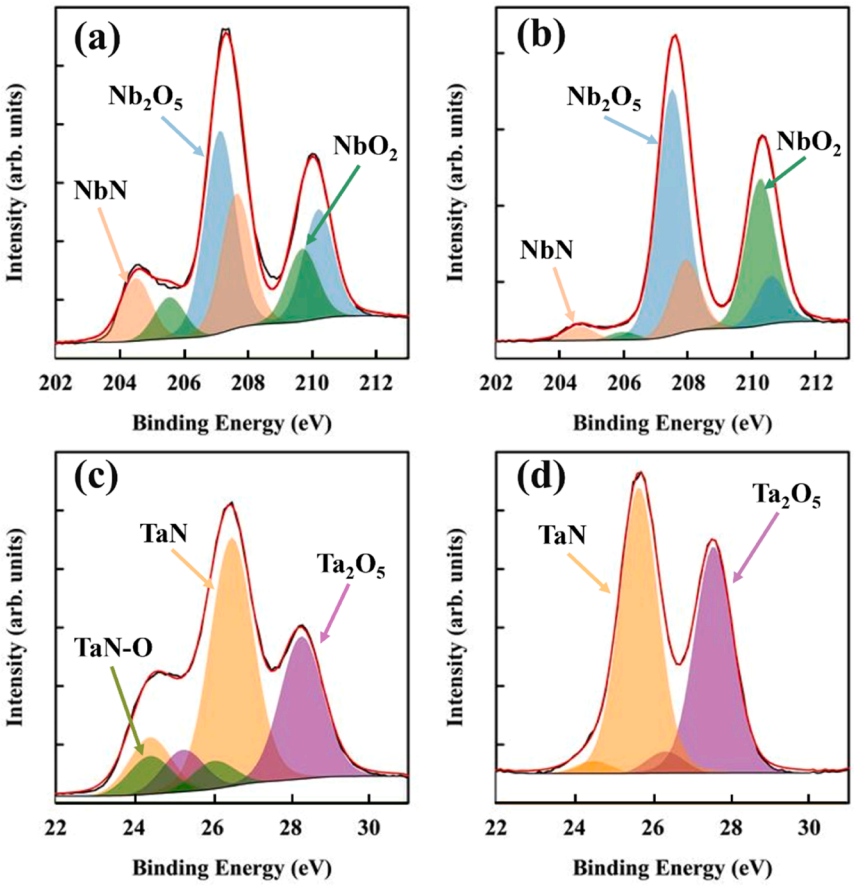

Fig. 10. X-ray photoelectron spectroscopy (XPS) analysis for NbN coating **(a)** before, **(b)** after CA, and for TaN coating **(c)** before, and **(d)** after CA.

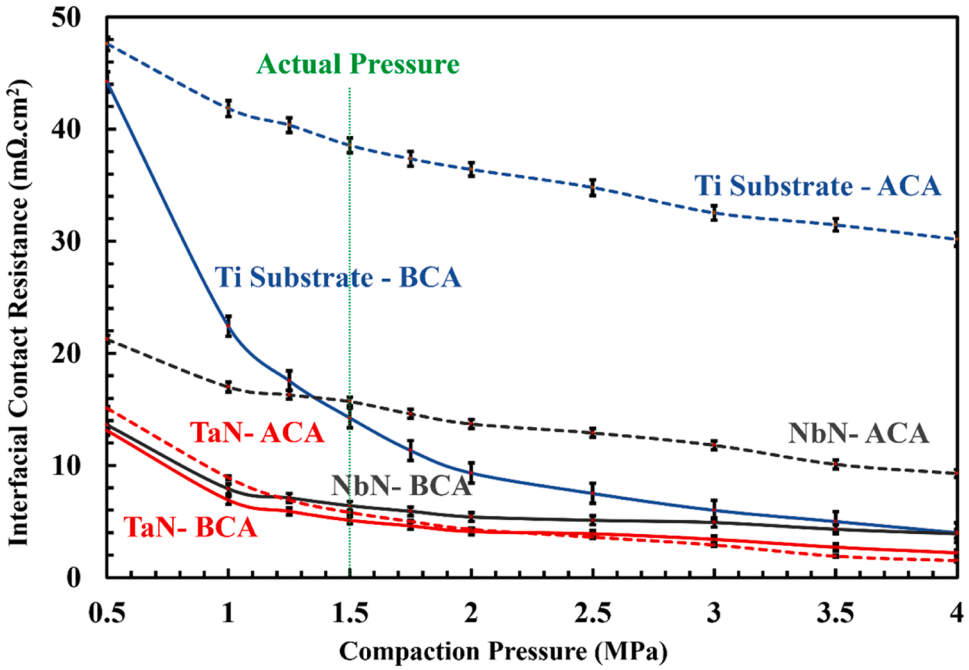

Fig. 11. ICR values of the Ti substrate and coated samples, before and after 6.0 h of CA polarization (dotted lines) in 0.5 M H_2SO_4 electrolyte at 70 °C. BCA and ACA represent ICR before and after the CA test, respectively.

~16 mΩ.cm^2 due to the formation of Nb oxide on the surface. TaN outperformed both Ti and NbN in terms of electrical conductivity and before CA test, the ICR was the lowest, around 6 mΩ.cm^2, demonstrating excellent electrical performance. Even after CA test, the ICR remained almost unchanged about 7 mΩ.cm^2, which was lower than 10 mΩ.cm^2 as the DOE technical target for BPPs in PEMFCs [91].

From the observations, it was clear that TaN exhibited the best overall performance by having the lowest increase in the ICR after CA test, making it the most stable and corrosion-resistant coating. The minimal change in ICR indicates that the continuous conductive pathways through the TaN sublayer remain intact, despite the oxide signal observed by XPS. NbN, although showed better conductivity compared to Ti, the degradation on the surface resulted in an increase in ICR. Ti substrate performed the worst, with a significant ICR increase, which confirmed the crucial need of protective coatings to prevent severe electrical and mechanical degradation. These findings suggest that TaN is the suitable coating for BPP for fuel cell applications, where maintaining low ICR under moderate compression is critical for efficiency and longevity.

3.5. Contact angle measurement

Water handling is critical to the performance and longevity of PEMFCs. Inadequate water handling by BPPs, particularly on the cathode side of the stack, can result in water accumulation in the cell by not being able to properly remove the water out of the cell [16]. Surface wettability, a key factor in water management, refers to how water interacts with the surface, influencing whether water tends to spread out (hydrophilic surface) or bead up (hydrophobic surface). By measuring the static contact angle, an insight into the interaction between the solid surface, liquid, and the surrounding air will be obtained [92]. Static contact angle measurements were performed prior to the electrochemical tests to evaluate and compare the wettability of the NbN- and TaN-coated surfaces with that of the bare Ti substrate. In general, increased hydrophobicity enhances the water management efficiency of titanium BPPs [93,94]. The contact angle measurement on the Ti substrate (Fig. 12 **(a)**) and coated substrates was done, and the results showed that for Ti the contact angle was around 80° while it increased to around 101.5° for NbN (Fig. 12 **(b)**), and 124.5° for TaN coatings. TaN coating (Fig. 12 **(c)**), applied on the surface, was able to increase the contact angle to very high values, which indicated the surface wettability changing from hydrophilic to hydrophobic. The bar chart of three measurements and the average for Ti substrate, NbN and TaN coatings are provided in Fig. 12 **(d)**.

Table 5 is intended to compare two key parameters defined by the DOE for bipolar plates (BPPs) in PEMFC applications, evaluated in this study alongside selected recent works from the literature, particularly those employing similar nitride-based coatings, in order to explain the advantage of using TaN coating applied by magnetron sputtering as a candidate coating for BPPs used in PEMFC. It can be seen that with using this coating in thickness scale lower than micrometer, the targets determined by DOE were achieved. The importance of introducing an interlayer such as TiN can be noticed in increasing the durability of transition metals nitride-based coatings. The usage of TA2 was also not

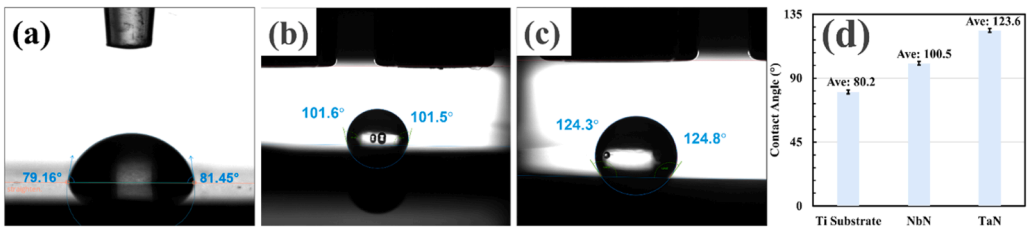

Fig. 12. Contact angle measurement of **(a)** Ti substrate, **(b)** NbN, and **(c)** TaN coated samples and (d) bar chart of the average measurements for contact angle.

Table 5
Comparison of i_{corr} and ICR (after corrosion tests) of the current work with similar research works in literature.

Substrate	Coating	Thickness (µm)	i_{corr} (µA.cm^{-2})	ICR after corr. test at 1.4–1.5 (mΩ.cm^2)	Reference
TA2 (Current work)	TaN	0.57	0.8	7.0	-
TA2 (Current work)	NbN	0.63	34.3	16.0	-
TA1	TiN	4.2	7.1	30.0	[19]
TA1	Ta/TaN	1.2	~5	-	[90]
TA1	Nb/NbN	1.0	3.0	~12.0*	[90]
TA1	Cr/CrN	0.6	-	31.0	[90]
TA1	TiN/CrN	5.1	9.4	8.5	[19]
TA5	TiNbN	2.2	0.03	9.6	[95]
TA1	TaN	~0.5*	0.3	-	[96]
TA2	CrN	0.57	0.15	8.8	[97]

* These values are estimates read from published figures

considered by these research works, while it was used in present study due to the proper properties mentioned earlier.

4. Conclusion

In this research, niobium-nitride (NbN) and tantalum-nitride (TaN) thin coatings were deposited on Ti-based substrate to investigate the potential usage of Ti-based bipolar plates (BPPs) in proton exchange membrane fuel cell (PEMFC) application. The nitride coatings enhanced the electrochemical stability and corrosion resistance of Ti BPPs in accelerated corrosive conditions defined by the U.S. Department of Energy (DOE). Potentiodynamic polarization plots revealed a corrosion current density (i_{corr}) of 0.8 µA.cm^{-2} for the TaN coated substrate, meeting the DOE target, while the NbN coated substrate exhibited a significantly higher i_{corr} of 34 µA.cm^{-2}, exceeding the target because of the enormous degradation of the coating After 6.0 h of chronoamperometry (CA) testing at 0.2 V vs. Hg/Hg_2SO_4, TaN and NbN coating displayed current densities of 0.67 µA.cm^{-2} and 7.93 µA.cm^{-2}, respectively. This comparative analysis indicates that although both coatings improved corrosion resistance, only TaN consistently satisfied the DOE requirements. When the applied voltage was increased to 0.8 V vs. Hg/Hg_2SO_4 to evaluate durability in a more oxidizing and corrosion-intensive condition, TaN-coated Ti BPPs exhibited excellent stability with a current density of ~0.06 mA.cm^{-2} over 6.0 h. In contrast, NbN showed progressive degradation with the current density surpassing, 0.30 mA.cm^{-2}. The surface morphology confirmed the superior stability of TaN, showing no significant surface damage, pitting, or delamination, while NbN coatings suffered from severe surface deterioration and delamination. These findings highlight TaN's ability to form a stable passive layer that effectively suppresses corrosion processes. In addition, interfacial contact resistance (ICR) measurements confirmed the electrochemical results, demonstrating that TaN maintained superior conductivity with negligible ICR increase after corrosion tests showing values around 7.0 mΩ.cm^2. In contrast, NbN exhibited higher ICR which was because of the degradation in the coating. Comparing the current work with the previous work using multilayer Nb/Ta coatings, shows that nitride of the Ta produced on the surface with magnetron sputtering can have equal effectiveness by using only one metallic target and with purging nitrogen in the system. In summary, TaN-coated Ti BPPs outperformed NbN in terms of corrosion resistance, durability, and electrical conductivity, meeting DOE targets. The favorable performance of TaN may be associated with its dense morphology, chemical stability, and stable passive film formation, contributing to its excellent corrosion resistance. Therefore, TaN is identified as a promising candidate coating for PEMFC bipolar plates.

CRediT authorship contribution statement

Xianguo Li: Writing – review & editing, Validation, Supervision, Project administration, Funding acquisition. **Abhay Gupta:** Writing – review & editing, Validation, Methodology, Formal analysis. **Samaneh Shahgaldi:** Writing – review & editing, Validation, Supervision, Project administration, Funding acquisition, Conceptualization. **Mohammadhossein Johar:** Writing – review & editing, Writing – original draft, Visualization, Validation, Software, Methodology, Investigation, Formal analysis, Data curation, Conceptualization. **Leila Moradizadeh:** Writing – original draft, Methodology, Formal analysis, Data curation. **Yasin Mehdizadeh Chellehbari:** Writing – original draft, Validation, Investigation, Formal analysis.

Declaration of Competing Interest

The authors declare that they have no known competing financial interests or personal relationships that could have appeared to influence the work reported in this paper.

Acknowledgment

Shahgaldi research team at the Hydrogen Research Institute, University of Quebec a Trois Rivières would like to acknowledge the support of the Natural Sciences and Engineering Research Council of Canada (NSERC), Canada Research Chair (CRC−2019–00354), Discovery grant (CRSNG-DGECR−2022–00058), NSERC-Alliance (ALLRP 571713–21) Prima Quebec (R23–13–005), and Mitacs Accelerate (IT30506). The authors would like to thank Niobay team for their constant support.

Data availability

Data will be made available on request.

References

[1] P.V. Madhavan, A. Amirsoleymani, S. Shahgaldi, X. Li, Data-driven multi-objective optimization of flow field header design for PEM fuel cells, Int. J. Hydrog. Energy 201 (2026) 153023, https://doi.org/10.1016/j.ijhydene.2025.153023.
[2] P.V. Madhavan, S. Anwar, S. Shahgaldi, X. Li, Diamond-like-carbon coated metallic bipolar plates for PEM Fuel cells: an assessment of coating thickness effect, Fuel Cells 25 (2025) e70036, https://doi.org/10.1002/fuce.70036.
[3] J. Li, L. Feng, H. Zhang, J. Zhang, A. Li, X. Yu, C. Wang, Properties of Cr–C films prepared by multi-point magnetron co-sputtering on 316L stainless steel using as bipolar plates for PEMFCs, Int. J. Hydrog. Energy 69 (2024) 1377–1385, https://doi.org/10.1016/j.ijhydene.2024.05.117.
[4] S. Shahgaldi, A. Ozden, X. Li, F. Hamdullahpur, A scaled-up proton exchange membrane fuel cell with enhanced performance and durability, Appl. Energy 268 (2020) 114956, https://doi.org/10.1016/j.apenergy.2020.114956.
[5] S. Shahgaldi, A. Ozden, X. Li, F. Hamdullahpur, A novel membrane electrode assembly design for proton exchange membrane fuel cells: Characterization and performance evaluation, Electrochim. Acta 299 (2019) 809–819, https://doi.org/10.1016/j.electacta.2019.01.064.
[6] A. Ozden, S. Shahgaldi, X. Li, F. Hamdullahpur, A review of gas diffusion layers for proton exchange membrane fuel cells—With a focus on characteristics, characterization techniques, materials and designs, Prog. Energy Combust. Sci. 74 (2019) 50–102, https://doi.org/10.1016/j.pecs.2019.05.002.
[7] M.C. Yasin, M. Johar, A. Gupta, S. Shahgaldi, A comprehensive review of the material innovations and corrosion mitigation strategies for PEMWE bipolar plates, Int. J. Hydrog. Energy 88 (2024) 726–747, https://doi.org/10.1016/j.ijhydene.2024.09.208.
[8] Y.Der Kuan, C.W. Ciou, M.Y. Shen, C.K. Wang, R.Z. Fitriani, C.Y. Lee, Bipolar plate design and fabrication using graphite reinforced composite laminate for proton exchange membrane fuel cells, Int. J. Hydrog. Energy 46 (2021) 16801–16814, https://doi.org/10.1016/j.ijhydene.2020.08.030.
[9] Q. Yin, K. Zhang, X.Z. Fu, X.Z. Wang, J.L. Luo, Rapid coating preparation strategy for chromium nitride coated titanium bipolar plates of proton exchange membrane fuel cells, Int. J. Hydrog. Energy 47 (2022) 31435–31445, https://doi.org/10.1016/j.ijhydene.2022.07.057.

[10] S.H. Wang, J. Peng, W.B. Lui, J.S. Zhang, Performance of the gold-plated titanium bipolar plates for the light weight PEM fuel cells, J. Power Sources 162 (2006) 486–491, https://doi.org/10.1016/j.jpowsour.2006.06.084.
[11] C.T.A. Sarjuni, A.A.D. Shahril, H.C. Low, B.H. Lim, Bipolar Plate Design Assessment: Proton Exchange Membrane Fuel Cell and Water Electrolyzer, Fuel Cells 24 (2024) e202300196, https://doi.org/10.1002/fuce.202300196.
[12] Y. Gou, H. Chen, R. Li, J. Geng, Z. Shao, Nb–Cr–C coated titanium as bipolar plates for proton exchange membrane fuel cells, J. Power Sources 520 (2022), https://doi.org/10.1016/j.jpowsour.2021.230797.
[13] N.F. Asri, T. Husaini, A.B. Sulong, E.H. Majlan, W.R.W. Daud, Coating of stainless steel and titanium bipolar plates for anticorrosion in PEMFC: A review, Int. J. Hydrog. Energy 42 (2017) 9135–9148, https://doi.org/10.1016/j.ijhydene.2016.06.241.
[14] Q. Yin, K. Zhang, X.Z. Fu, X.Z. Wang, J.L. Luo, Rapid coating preparation strategy for chromium nitride coated titanium bipolar plates of proton exchange membrane fuel cells, Int. J. Hydrog. Energy 47 (2022) 31435–31445, https://doi.org/10.1016/j.ijhydene.2022.07.057.
[15] Y. Mehdizadeh Chellehbari, P.V. Madhavan, M. Johar, L. Moradizadeh, A. Gupta, X. Li, S. Shahgaldi, Machine learning-assisted optimization of NbTa alloy coating thickness via DC magnetron sputtering for SS316L bipolar plates in PEMFCs, ETransportation 26 (2025) 100500, https://doi.org/10.1016/j.etran.2025.100500.
[16] M. Johar, L. Moradizadeh, A. Gupta, Y. Mehdizadeh Chellehbari, X. Li, S. Shahgaldi, Development of novel Nb and Ta multilayer coatings for corrosion protection of Ti-based bipolar plates for proton exchange membrane fuel cells, Corros. Sci. 245 (2025), https://doi.org/10.1016/j.corsci.2025.112707.
[17] S. Stiber, M. Hehemann, M. Carmo, M. Müller, K.E. Ayers, C. Capuano, N. Danilovic, T. Morawietz, I. Biswas, P. Gazdzicki, J.F. Heger, A.S. Gago, K. A. Friedrich, Long-Term Operation of Nb-Coated Stainless Steel Bipolar Plates for Proton Exchange Membrane Water Electrolyzers, Adv. Energy Sustain. Res. 3 (2022), https://doi.org/10.1002/aesr.202200024.
[18] H.S. Choi, D.H. Han, W.H. Hong, J.J. Lee, Titanium, chromium) nitride coatings for bipolar plate of polymer electrolyte membrane fuel cell, J. Power Sources 189 (2009) 966–971, https://doi.org/10.1016/j.jpowsour.2008.12.060.
[19] H. Cheng, H. Luo, X. Wang, Z. Pan, Q. Zhao, C. Dong, X. Li, Improving the performance of titanium bipolar plate in proton exchange membrane water electrolysis environment by nitrogen-chromium composite cathode plasma electrolytic deposition, Int. J. Hydrog. Energy 48 (2023) 38557–38568, https://doi.org/10.1016/j.ijhydene.2023.06.177.
[20] L. Jing, J. Wu, L. Chang, X. Lu, X. Li, L. Li, L. Ma, J. Hao, G. Zhang, Z. Deng, J. Yao, D. Jing, Effects of DC pulse mode on the performance of nitride coatings: a case study of NbN coatings, Appl. Surf. Sci. 714 (2025) 164398, https://doi.org/10.1016/j.apsusc.2025.164398.
[21] A. Bend, V.A.S. Kandadai, J.B. Petersen, B.K. Jasthi, Effect of deposition pressure on the microstructure, mechanical, and corrosion properties of tantalum nitride thin films deposited by reactive pulsed laser deposition, Vacuum 238 (2025) 114228, https://doi.org/10.1016/j.vacuum.2025.114228.
[22] G. Bräuer, B. Szyszka, M. Vergöhl, R. Bandorf, Magnetron sputtering - Milestones of 30 years. in: Vacuum, Elsevier Ltd, 2010, pp. 1354–1359, https://doi.org/10.1016/j.vacuum.2009.12.014.
[23] Y. Chen, J. Xu, Z.-H. Xie, P. Munroe, Nanocrystalline TaCN coated titanium bipolar plate dedicated to proton exchange membrane fuel cell, Ceram. Int. 48 (2022) 19217–19231, https://doi.org/10.1016/j.ceramint.2022.03.214.
[24] A. Srivastava, K.A. Ross, C.B. Smith, Coating developments towards enabling aluminum as a bipolar plate material for PEM fuel cells, J. Power Sources 582 (2023) 233513, https://doi.org/10.1016/j.jpowsour.2023.233513.
[25] M.A. Baker, S.J. Greaves, E. Wendler, V. Fox, A comparison of in situ polishing and ion beam sputtering as surface preparation methods for XPS analysis of PVD coatings, 2000. https://doi.org/10.1016/S0040-6090(00)01272-4.
[26] Z.J. Wu, R.L. Liu, Z.H. Liu, X.Y. Wu, F.L. Li, Microstructure and property of multilayer TiN/TiCN nanocrystalline coating used for metal bipolar plate, Vacuum 227 (2024), https://doi.org/10.1016/j.vacuum.2024.113361.
[27] J.F. Tang, C.H. Huang, C.Y. Lin, F.C. Yang, C.L. Chang, Effects of substrate rotation speed on structure and adhesion properties of CrN/CrAlSiN multilayer coatings prepared using high-power impulse magnetron sputtering, Coatings 10 (2020), https://doi.org/10.3390/COATINGS10080742.
[28] J.E. Alfonso, J. Buitrago, J. Torres, J.F. Marco, B. Santos, Influence of fabrication parameters on crystallization, microstructure, and surface composition of NbN thin films deposited by rf magnetron sputtering, J. Mater. Sci. 45 (2010) 5528–5533, https://doi.org/10.1007/s10853-010-4612-3.
[29] Y.P. Dahal, B. Gu, Z. Su, S. Wang, Investigating the effect of sputtering particle energy on the crystal orientation and microstructure of NbN thin films, Coatings 15 (2025) 460, https://doi.org/10.3390/coatings15040460.
[30] S.-I. Baik, Y.-W. Kim, Microstructural evolution of tantalum nitride thin films synthesized by inductively coupled plasma sputtering, Appl. Microsc. 50 (2020) 7, https://doi.org/10.1186/s42649-020-00026-7.
[31] L. Moradizadeh, M. Johar, Y.M. Chellehbari, X. Li, S. Shahgaldi, Optimized tantalum interlayer thickness for PTLs: Enhancing PEMWE performance, stability, and reducing precious metal loading, J. Power Sources 647 (2025) 237360, https://doi.org/10.1016/j.jpowsour.2025.237360.
[32] A. Chen, J. Jiang, X. Li, J. Hou, Z. Ding, B. Gan, K. Zhang, Formation and effect of hierarchical structures on corrosion performance of stainless steel bipolar plate fabricated by powder bed fusion, Corros. Sci. 219 (2023), https://doi.org/10.1016/j.corsci.2023.111193.
[33] X. Ma, T. Wang, B. Gong, H. Cao, Fast and low-cost deposition strategy for constructing amorphous carbon layer toward corrosion protection on aluminum alloy bipolar plates in proton exchange membrane fuel cell environments, J. Power Sources 623 (2024), https://doi.org/10.1016/j.jpowsour.2024.235479.
[34] P. Varsan Madhavan, S. Shahgaldi, X. Li, Ex-situ Characterization of Nb-Ti Alloy/Pt Coated Stainless Steel Bipolar Plates for Proton Exchange Membrane Fuel Cells, Energy Convers. Manag. 311 (2024), https://doi.org/10.1016/j.enconman.2024.118536.
[35] A.E. Fetohi, R.M. Abdel Hameed, K.M. El-Khatib, E.R. Souaya, Study of different aluminum alloy substrates coated with Ni-Co-P as metallic bipolar plates for PEM fuel cell applications, Int. J. Hydrog. Energy 37 (2012) 10807–10817, https://doi.org/10.1016/j.ijhydene.2012.04.066.
[36] W. Li, L. Liu, Y. Wang, H. Li, Z. Li, Evaluation of vacuum heat-treated α-C films for surface protection of metal bipolar plates used in polymer electrolyte membrane fuel cells, Int. J. Hydrog. Energy 46 (2021) 22983–22997, https://doi.org/10.1016/j.ijhydene.2021.04.132.
[37] H. Cheng, H. Luo, X. Wang, C. Dong, X. Li, Effect of fluoride ion concentration and fluctuating conditions on titanium bipolar plate in PEM water electrolyser environment, Corros. Sci. 222 (2023), https://doi.org/10.1016/j.corsci.2023.111414.
[38] M. Ahangari, M.H. Johar, M. Saremi, Hydroxyapatite-carboxymethyl cellulose-graphene composite coating development on AZ31 magnesium alloy: Corrosion behavior and mechanical properties, Ceram. Int. 47 (2021) 3529–3539, https://doi.org/10.1016/j.ceramint.2020.09.197.
[39] B.R. Hinderliter, S.G. Croll, D.E. Tallman, Q. Su, G.P. Bierwagen, Interpretation of EIS data from accelerated exposure of coated metals based on modeling of coating physical properties, Electrochim. Acta 51 (2006) 4505–4515, https://doi.org/10.1016/j.electacta.2005.12.047.
[40] B. Normand, H. Takenouti, M. Keddam, H. Liao, G. Monteil, C. Coddet, Electrochemical impedance spectroscopy and dielectric properties of polymer: application to PEEK thermally sprayed coating. Electrochimica Acta, 2004, pp. 2981–2986, 10.1016/j.electacta.2004.01.057.
[41] G.W. Walter, A review of impedance plot methods used for corrosion performance analysis of painted metals, Corros. Sci. 26 (1986) 681–703, https://doi.org/10.1016/0010-938X(86)90033-8.
[42] Y. Zhang, A. Poursaee, Study of the semi-conductive behavior of the passive film on carbon steel in simulated concrete pore solution under stress, Anti-Corros. Methods Mater. 62 (2015) 363–370, https://doi.org/10.1108/ACMM-04-2014-1375.
[43] A. Kraytsberg, M. Auinat, Y. Ein-Eli, Reduced contact resistance of PEM fuel cell's bipolar plates via surface texturing, J. Power Sources 164 (2007) 697–703, https://doi.org/10.1016/j.jpowsour.2006.11.033.
[44] L. Ward, A. Pilkington, S. Dowey, Studies on the effect of arc current mode and substrate rotation configuration on the structure and corrosion behavior of PVD TiN coatings, Coatings 7 (2017) 50, https://doi.org/10.3390/coatings7040050.
[45] D.K. Merl, P. Panjan, M. Panjan, M. Čekada, The role of surface defects density on corrosion resistance of PVD hard coatings, Plasma Process. Polym. 4 (2007) S613–S617, https://doi.org/10.1002/ppap.200731416.
[46] W.D. Sproul, Physical vapor deposition tool coatings, Surf. Coat. Technol. 81 (1996) 1–7, https://doi.org/10.1016/0257-8972(95)02616-9.
[47] J.J. Zhang, X. Su, L. Zhang, L. Zheng, X.F. Wang, L. You, Improvement of the superconducting properties of NbN thin film on single-crystal silicon substrate by using a TiN buffer layer, Supercond. Sci. Technol. 26 (2013) 45010, https://doi.org/10.1088/0953-2048/26/4/045010.
[48] R.F. Bunshah, C. Weissmantel, Handbook of hard coatings, Noyes Publications, Park Ridge, NJ, 2001.
[49] M.A. Iqbal, S. Singh, A. Singh, S. Shahgaldi, Enhancing durability of Pt-coated titanium porous transport layers for PEM water electrolysis using TiN interlayers, Mater. Adv. (2026), https://doi.org/10.1039/D5MA01378J.
[50] E. Mohseni, E. Zalnezhad, A.R. Bushroa, Abdel Magid Hamouda, B.T. Goh, G. H. Yoon, Ti/TiN/HA coating on Ti–6Al–4V for biomedical applications, Ceram. Int. 41 (2015) 14447–14457, https://doi.org/10.1016/j.ceramint.2015.07.081.
[51] C.-H. Hsu, C.-Y. Lin, J.-X. Chen, Wear and Corrosion Performance of Ti-6Al-4V Alloy Arc-Coated TiN/CrN Nano-Multilayer Film, Met. (Basel) 13 (2023), https://doi.org/10.3390/met13050907.
[52] J. Chen, S. Zhang, J. Zheng, Y. Dong, C. Zhang, J. Li, Z. Chen, J. Zhang, D. Sun, Excellent anti-corrosion and conductivity of NbN coated on Ti bipolar plate by controlling N2 flow rates, J. Alloy. Compd. 976 (2024), https://doi.org/10.1016/j.jallcom.2023.173033.
[53] Y. Lou, Y. Wang, K. Zhang, J. Li, Y. Wu, D. Gao, Y. Li, H. Wang, Z. Shen, X. Zeng, Dissolution-Driven Phase Transformation and Precipitation in a FeCrNiAl Dual-Phase HEA Exposed to Oxygen-Deficient LBE, Corros. Sci. (2026) 113624, https://doi.org/10.1016/j.corsci.2026.113624.
[54] H. Cheng, H. Luo, X. Wang, C. Dong, X. Li, Effect of fluoride ion concentration and fluctuating conditions on titanium bipolar plate in PEM water electrolyser environment, Corros. Sci. 222 (2023), https://doi.org/10.1016/j.corsci.2023.111414.
[55] Y. Zhou, K. Chen, Y. You, X. Shang, Y. Li, H. Shi, J. Dang, K. Zhang, S. Lozano-Perez, L. Zhang, Oxide stress and fracture susceptibility on a surface gradient microstructure of an additively manufactured steel, Acta Mater. (2025) 121779, https://doi.org/10.1016/j.actamat.2025.121779.
[56] F. Cai, Q. Zhou, J. Chen, S. Zhang, Effect of inserting the Zr layers on the tribo-corrosion behavior of Zr/ZrN multilayer coatings on titanium alloys, Corros. Sci. 213 (2023), https://doi.org/10.1016/j.corsci.2023.111002.
[57] M.H. Johar, H. Torbati-Sarraf, M. Ahangari, M. Saremi, Inhibiting effect of Benzotriazole on the stress corrosion cracking of Cu-27%Ni cupronickel and Cu-30%Zn brass in Mattsson's solution, Mater. Lett. 293 (2021), https://doi.org/10.1016/j.matlet.2021.129735.

[58] Y. Wang, S. Zhang, Z. Lu, L. Wang, W. Li, Preparation and performances of electrically conductive Nb-doped TiO2 coatings for 316 stainless steel bipolar plates of proton-exchange membrane fuel cells, Corros. Sci. 142 (2018) 249–257, https://doi.org/10.1016/j.corsci.2018.07.034.
[59] A. Gupta, C. Srivastava, Low-temperature Sn electrodeposition: Texture evolution, grain boundary constitution and corrosion behavior, Surf. Coat. Technol. 425 (2021), https://doi.org/10.1016/j.surfcoat.2021.127709.
[60] A. Gupta, C. Srivastava, Electrodeposition current density induced texture and grain boundary engineering in Sn coatings for enhanced corrosion resistance, Corros. Sci. 194 (2022), https://doi.org/10.1016/j.corsci.2021.109945.
[61] Y. Chen, Y. Liu, T. Ying, Y. Yang, J. Wang, X. Xu, Z. Shen, Y. Li, D. Qiu, H. Zhu, Stainless magnesium alloy based on self-healing amorphous surface, Mater. Today (2025), https://doi.org/10.1016/j.mattod.2025.11.015.
[62] F. Mansfeld, Electrochemical impedance spectroscopy (EIS) as a new tool for investigating methods of corrosion protection, Electrochim. Acta 35 (1990) 1533–1544, https://doi.org/10.1016/0013-4686(90)80007-B.
[63] Z. Ma, L. Luo, J. Tan, S. Li, M. Pan, A novel Ta/TaN/TaAlN nanocrystalline coatings on metal bipolar plates with excellent corrosion resistance, J. Power Sources 632 (2025) 236307, https://doi.org/10.1016/j.jpowsour.2025.236307.
[64] H.C. Low, B.H. Lim, M.S. Masdar, M.I. Rosli, Understanding the factors influencing the corrosion of bipolar plate to the performance and durability of unitized regenerative proton exchange membrane fuel cell: A review, Int. J. Hydrog. Energy 57 (2024) 420–430, https://doi.org/10.1016/j.ijhydene.2024.01.010.
[65] A. Gupta, S. Shahgaldi, Effect of Nb interlayer thickness on the performance of porous transport layers for proton exchange membrane water electrolyzers, Renew. Energy (2026) 125373, https://doi.org/10.1016/j.renene.2026.125373.
[66] W.B. Utomo, S.W. Donne, Electrochemical behaviour of titanium in H2SO4–MnSO4 electrolytes, Electrochim. Acta 51 (2006) 3338–3345, https://doi.org/10.1016/j.electacta.2005.09.031.
[67] L. Chen, J. Lv, R. Liu, P. Yang, B. Zhang, Enhanced corrosion resistance of LaBC film for bipolar plate coatings in proton exchange membrane fuel cells, Diam. Relat. Mater. 148 (2024), https://doi.org/10.1016/j.diamond.2024.111458.
[68] Z. Zhang, M. Chen, G. Gyawali, T.F. Zhang, S. Zhang, Effect of nitrogen pressure on the microstructure, conductivity, and corrosion resistance of ZrN-coated stainless steel as bipolar plate for proton exchange membrane fuel cell, Ceram. Int. (2024), https://doi.org/10.1016/j.ceramint.2024.08.315.
[69] Y. Mehdizadeh Chellehbari, L. Moradizadeh, M. Johar, A. Gupta, X. Li, S. Shahgaldi, Evaluation of niobium-based bipolar plates with ultra-low precious metal coatings for high-performance and durable PEM water electrolyzers, Mater. Today Energy 51 (2025) 101913, https://doi.org/10.1016/j.mtener.2025.101913.
[70] F.C. Silva, O.M. Prada Ramirez, M.A. Tunes, P.D. Edmondson, J.C. Sagás, L. C. Fontana, H.G. de Melo, C.G. Schön, Corrosion resistance of functionally graded TiN/Ti coatings for proton exchange membrane fuel cells, Int. J. Hydrog. Energy 45 (2020) 33993–34010, https://doi.org/10.1016/j.ijhydene.2020.09.037.
[71] P. Zhang, C. Hao, Y. Han, F. Du, H. Wang, X. Wang, J. Sun, Electrochemical behavior and surface conductivity of NbC modified Ti bipolar plate for proton exchange membrane fuel cell, Surf. Coat. Technol. 397 (2020) 126064, https://doi.org/10.1016/j.surfcoat.2020.126064.
[72] Q. Shen, M. Hou, D. Liang, Z. Zhou, X. Li, Z. Shao, B. Yi, Study on the processes of start-up and shutdown in proton exchange membrane fuel cells, J. Power Sources 189 (2009) 1114–1119, https://doi.org/10.1016/j.jpowsour.2008.12.075.
[73] L. Li, T. Tokoroyama, R. Zhang, N. Umehara, Corrosion and tribological properties of ta-C/ta-C: Ta coatings: Analysis of the influence of Ta-O/Ta-C ratio, Tribol. Int. 198 (2024), https://doi.org/10.1016/j.triboint.2024.109916.
[74] A. Robin, J.L. Rosa, Corrosion behavior of niobium, tantalum and their alloys in hot hydrochloric and phosphoric acid solutions, n.d. https://doi.org/10.1016/S0263-4368(99)00034-7.
[75] K. Chen, Y. Zhou, Z. Shen, L. Zhang, F. Scenini, X. Zeng, S. Lozano-Perez, Insights into the complexities of diffusion-induced grain boundary migration in Fe-Cr-Ni ternary alloys, Acta Mater. (2025) 121836, https://doi.org/10.1016/j.actamat.2025.121836.
[76] A. Kumar, G. Malik, R. Adalati, V. Chawla, M.K. Pandey, R. Chandra, Tuning the wettability of highly transparent Nb2O5 nano-sliced coatings to enhance anti-corrosion property, Mater. Sci. Semicond. Process. 123 (2021), https://doi.org/10.1016/j.mssp.2020.105513.
[77] H.B. Nie, S.Y. Xu, S.J. Wang, L.P. You, Z. Yang, C.K. Ong, J. Li, T.Y.F. Liew, Structural and electrical properties of tantalum nitride thin films fabricated by using reactive radio frequency magnetron sputtering, n.d. https://doi/org/10.1007/s003390000691.
[78] E. Nurlaela, A. Ziani, K. Takanabe, Tantalum nitride for photocatalytic water splitting: concept and applications, Mater. Renew. Sustain. Energy 5 (2016), https://doi.org/10.1007/s40243-016-0083-z.
[79] Y. Leng, D. Yang, P. Ming, C. Zhang, A comparative study of corrosion resistance evaluation of bipolar plate materials for proton exchange membrane fuel cell, ETransportation 10 (2021), https://doi.org/10.1016/j.etran.2021.100139.
[80] J. Zhang, J. Jin, Y. Tao, R. Cao, X. Kou, X. Tian, Investigation of corrosion properties with Ni–P/TiNO coating on aluminum alloy bipolar plates in proton exchange membrane fuel cell, Int. J. Hydrog. Energy 47 (2022) 22165–22179, https://doi.org/10.1016/j.ijhydene.2022.05.024.
[81] J.E. Cotter, J.H. Guo, P.J. Cousins, M.D. Abbott, F.W. Chen, K.C. Fisher, P-type versus n-type silicon wafers: prospects for high-efficiency commercial silicon solar cells, IEEE Trans. Electron. Devices 53 (2006) 1893–1901, https://doi.org/10.1109/TED.2006.878026.
[82] S. Song, S. Peng, C. Zhang, Q. Wu, X. Cui, Y. Zhao, X. Wang, D. Sun, Optimization of tantalum nitride coatings for fuel cell bipolar plates: balancing corrosion resistance and electrical conductivity through phase composition tuning, Int. J. Hydrog. Energy 140 (2025) 407–419, https://doi.org/10.1016/j.ijhydene.2025.05.181.
[83] A.D. Schneider, P.S. Boeck, G. Copetti, T.J.A. Mori, R.D. Della Pace, L.F. Schelp, L. S. Dorneles, Crystallographic texture evolution in NbN thin films produced by reactive magnetron sputtering, Thin Solid. Films (2025) 140816, https://doi.org/10.1016/j.tsf.2025.140816.
[84] S. Lv, K. Li, Semiconducting behaviour and corrosion resistance of passive film on corrosion-resistant steel rebars, Materials 15 (2022), https://doi.org/10.3390/ma15217644.
[85] J. Cheng, J. Xu, L.L. Liu, S. Jiang, Electrochemical corrosion behavior of Ta2n nanoceramic coating in simulated body fluid, Materials 9 (2016), https://doi.org/10.3390/ma9090772.
[86] G. Liu, D. Shan, B. Fang, X. Wang, Novel hybrid coating of TiN and carbon with improved corrosion resistance for bipolar plates of PEM water electrolysis, Int. J. Hydrog. Energy 48 (2023) 18996–19007, https://doi.org/10.1016/j.ijhydene.2023.02.015.
[87] B. Mi, T. Chen, J. Zhang, X. Ma, J. Wang, P. Liu, H. Wang, W. Li, Effect of N doping on Cr-doped amorphous carbon /CrN /Ti multilayer coatings on 316L stainless steel bipolar plate for PEMFC: First principles calculation, structure and performance, Int. J. Hydrog. Energy 71 (2024) 1303–1316, https://doi.org/10.1016/j.ijhydene.2024.05.294.
[88] S. Li, R. Jin, S. Li, L. Wang, Z. Xie, X. Li, Z. Wang, High corrosion resistance and conductivity of Al2O3/CrN coating for metal bipolar plates in PEMFCs: Al2O3 hinders CrN columnar crystals growth, Int. J. Hydrog. Energy 50 (2024) 805–816, https://doi.org/10.1016/j.ijhydene.2023.09.052.
[89] W. Yan, Y. Zhang, L. Chen, J. Luo, P. Pang, X. Zhang, B. Liao, M. Ying, Corrosion behavior and interfacial conductivity of amorphous hydrogenated carbon and titanium carbide composite (a-C: H/TiC) films prepared on titanium bipolar plates in PEMFCs, Diam. Relat. Mater. 120 (2021), https://doi.org/10.1016/j.diamond.2021.108628.
[90] H. Ye, Z. Tu, S. Li, Electrochemical performance of metal nitride coated titanium bipolar plate for proton exchange membrane water electrolyser, J. Power Sources 595 (2024), https://doi.org/10.1016/j.jpowsour.2024.234052.
[91] N. Saadat, H.N. Dhakal, J. Tjong, S. Jaffer, W. Yang, M. Sain, Recent advances and future perspectives of carbon materials for fuel cell, Renew. Sustain. Energy Rev. 138 (2021), https://doi.org/10.1016/j.rser.2020.110535.
[92] Y. Mehdizadeh Chellehbari, A. Gupta, X. Li, S. Shahgaldi, Impact of Surface Pretreatment on the Corrosion Resistance and Adhesion of Thin Film Coating on SS316L Bipolar Plates for Proton-Exchange Membrane Fuel Cell Applications, Molecules 29 (2024) 4319, https://doi.org/10.3390/molecules29184319.
[93] P. Gao, Z. Xie, X. Wu, C. Ouyang, T. Lei, P. Yang, C. Liu, J. Wang, T. Ouyang, Q. Huang, Development of Ti bipolar plates with carbon/PTFE/TiN composites coating for PEMFCs, Int. J. Hydrog. Energy 43 (2018) 20947–20958, https://doi.org/10.1016/j.ijhydene.2018.09.046.
[94] J. Shi, P. Zhang, Y. Han, H. Wang, X. Wang, Y. Yu, J. Sun, Investigation on electrochemical behavior and surface conductivity of titanium carbide modified Ti bipolar plate of PEMFC, Int. J. Hydrog. Energy 45 (2020) 10050–10058, https://doi.org/10.1016/j.ijhydene.2020.01.203.
[95] Y. Li, L. Zhang, M. Zhang, Z. Han, H. Chen, X. Liu, J. Zheng, Enhanced corrosion resistance and conductivity of TiNbN films on titanium alloy bipolar plates by tailoring nitrogen flow rate during magnetron sputtering, Surf. Coat. Technol. 528 (2026) 133414, https://doi.org/10.1016/j.surfcoat.2026.133414.
[96] J. Chen, S. Zhang, J. Li, Z. Chen, D. Sun, Effects of phase transformation on the corrosion resistance and conductivity of NbN coatings for metal bipolar plates, Surf. Coat. Technol. 497 (2025) 131800, https://doi.org/10.1016/j.surfcoat.2025.131800.
[97] Q. Yin, K. Zhang, X.-Z. Fu, X.-Z. Wang, J.-L. Luo, Rapid coating preparation strategy for chromium nitride coated titanium bipolar plates of proton exchange membrane fuel cells, Int. J. Hydrog. Energy 47 (2022) 31435–31445, https://doi.org/10.1016/j.ijhydene.2022.07.057.